Coronagraphic observations of the lunar sodium exosphere 2018–2019

R.M. Killen [a,*], T.H. Morgan [a], A.E. Potter [b], Giovanni Bacon [c], Irima Ajang [d], Andrew R. Poppe [e]

[a] NASA Goddard Space Flight Center, Solar System Exploration Division, Greenbelt, MD 20771, USA
[b] National Solar Observatory, Prescott, AZ 86301, Emeritus, USA
[c] Embry-Riddle Aeronautical University, Daytona Beach, FL 32114, USA
[d] Howard University, Washington, DC 20059, USA
[e] Space Sciences Laboratory, Univ. California Berkeley, Berkeley, CA 94720, USA

A B S T R A C T

Remote observations of the lunar sodium corona have been obtained with the Goddard Lunar Coronagraph located at the Winer Observatory in Sonoita, Arizona. We previously reported the results of observations in the spring, 2017, observing season (Killen et al., 2019). We report herein the results of the 2018–2019 observing campaign. We show definitive effects on the corona - the extended lunar sodium exosphere above 150 km from the surface - of enhanced ion flux onto the Moon as measured by the ARTEMIS ElectroStatic Analyzer. The three observations in this dataset with the largest column abundances are associated with entrance of the Moon into the magnetosheath. The enhancement in the exosphere due to ion flux is not long-lived after the enhanced ion influx decreases, confirming the findings of Killen et al., 2012. The column abundance is greatest at both the dawn and dusk terminators as predicted and simulated by Smyth and Marconi, 1995. The cause of the increased scale height at the terminators is consistent with radiation pressure acceleration anti-sunward. We report a shallow decline of column abundance with increasing latitude which is also consistent with radiation pressure acceleration. Most of our measured scale heights are on the order of 800–1800 km, increasing at high latitudes, consistent with the data set published in Killen et al., 2019. Although the intensity extrapolated to the surface decreases with latitude, the scale height increases with latitude, so that the exospheric column decreases more slowly with increasing latitude than does a cosine function.

1. Introduction

The source and loss processes of the lunar sodium exosphere, with implications for all surface-bounded exospheres, have been debated since the discovery of the exospheric Na in the 1980s. Although three processes - ion-sputtering, impact vaporization, and photon-stimulated desorption - have been demonstrated to be able to desorb or violently eject atoms from exposed surfaces across the solar system, the relative importance of these processes has been debated and is not resolved. At the same time the loss rate depends not only on the source process and its energetics, but also on the interaction of atoms that re-impact the surface after their initial ejection from the regolith. Previously, observations of the lunar sodium exosphere have been limited both temporally and spatially. As a consequence, models have been produced to fit an incomplete picture of exospheric behavior under different conditions. The ability to observe the entire exosphere at all latitudes and local times, and also through many lunations, is the goal of this project. Only

with a comprehensive dataset with good temporal and spatial coverage out to at least one lunar radius from the surface, can a realistic determination of the source and loss processes be made. These results have important implications for the true rates of these processes across the solar system.

In order to observe the lunar sodium exosphere out to one degree from the apparent center of the Moon, we designed, built and installed a small robotically controlled coronagraph at the Winer Observatory in Sonoita, Arizona. The description of the instrument, data acquisition, and data reduction procedure are discussed in Killen et al., 2019, but a brief description is given here. A lunar coronagraph was custom-designed by Claude Plymate and Roy Tucker and attached to a 101 mm refracting telescope which is operated remotely using The SkyX™ Professional software from Software Bisque. A 1.5 Å bandpass filter centered at 588.995 nm measures the sodium D_2 line and a 1.5 Å bandpass offband filter centered 3 Å blueward of the onband filter measures the continuum. An energy level diagram for the ground-state

---

and first excited states of the Na atom resulting in the D lines can be found in Chamberlain and Hunten (1987), p. 295.

The lunar sodium corona is very faint relative to the reflected light from the surface. Therefore we place an occulting disk over the image of the Moon. The coronagraph can carry 7 different possible occulting disks, including an open disk, designed to match the varying angular size of the Moon as seen from Earth. Our observations were obtained from approximately 143 km off the lunar surface to about one lunar radius above the surface, 1738 km. The autoguiding is performed with the SkyX™ autoguiding software by centering the guide camera on a bright crater and locking on for the duration of the evening. All images are therefore registered. Calibration is performed using the Hapke reflectance and observations of the lunar disk. We only observe on nights that are free of clouds or cirrus, which would cause random variations in our observations.

2. Data for the 2018–2019 observing seasons

We present limb profiles from the south pole to the north pole for many lunar phases. Because we observe over the illuminated limb, the local time at the limb is a function of the lunar phase angle (PA). For waning phase angles (Full Moon to New Moon) less than 90° the bright limb is in the morning, whereas for waning phases greater than 90° the bright limb is in the afternoon. The time of day flips for the waxing phases (from New Moon to Full Moon). Waxing phases greater than 90° show the bright morning limb, while waxing phases less than 90° show the afternoon limb. We report data according to whether the phases are waxing or waning because a different part of the lunar surface is visible for these different phases. Phases are illustrated in the Appendix (Fig. A1). We assume that PA is the Sun-Target-Observer angle, which only differs from the true phase angle at the sub-arcsec level, an unimportant difference for the Moon. An example of an observation of the lunar corona with the occulting disk covering the lunar disk, along with the superimposed image of the Moon taken directly after the occulted exposure, is shown in Fig. 1a. Fig. 1b shows the polar transformation of this image that we use to measure density and scale height as a function of latitude and altitude. Imperfections in the field and sensitivity are corrected with LED flats and sodium flats.

Table 1 lists the waning phases we observed in 2018, along with the phase angle, local time at the limb, the date, column abundance at the equator, the location of the peak column abundance, and the color in Fig. 2; Table 2 lists the same information for the waxing phases we observed in 2018, shown in Fig. 3. Table 3 lists the data for the 2019 observations (Fig. 4), and Table 4 lists the dates of high ion flux along

Table 1
Data for waning phases 2018.

Date (2018)	Phase angle	Local time at limb	Col. abund. equator (cm^{-2})	Peak col. abund. (cm^{-2})	Location peak (latitude)	Color in Fig. 2
Feb. 5	59	9:56	5.0×10^9	5.2×10^9	+20	magenta
Feb. 7	82	11:24	3.3×10^9	3.6×10^9	+20	orange
Mar. 3	14	7:00	1.7×10^{10}	1.8×10^{10}	±40	aqua
Apr 5	54	9:36	2.5×10^9	2.7×10^9	+20	green
May 8	88	11:52	1.7×10^9	2.7×10^9	−40	blue
Oct. 28	42	9:12	4.4×10^8	5.7×10^8	−40	black
Nov. 27	50	9:20	3.9×10^9	4.6×10^9	−40	red
Dec. 2	115	13:40	1.6×10^8	2.1×10^8	−80	purple

with the phase angle, derived zenith column abundances, ion flux to the lunar surface, and waxing or waning phase.

The dayside zenith column abundances of lunar sodium at the limb observed in 2018 for waning phases are plotted vs. latitude in Fig. 2(a), along with the local times at the limb. The observations are shown as solid lines because the observation is continuous, while the asterisks are a cosine function normalized to the observation at the equator. Fig. 2(b) plots scale heights vs. latitude for the same dates as Fig. 2(a). Fig. 3(a) shows dayside column abundances of lunar sodium at the limb (solid lines) for waxing phases for 2018 data, while Fig. 3(b) shows the corresponding scale heights. Fig. 4(a) shows dayside column abundances for spring 2019 and Fig. 4(b) shows the corresponding scale heights as a function of latitude and local time. Only one 2019 observation, June 15 at 16:08 local time, was a waxing phase. Others are waning phases. The scale height data were smoothed in IDL using a smoothing factor of 3.

3. Results and discussion

3.1. Results

We report herein on observations taken during spring and fall 2018, and spring, 2019. The data were reduced following procedures given in Killen et al., 2019. A different pattern of Mare and Highlands is at the
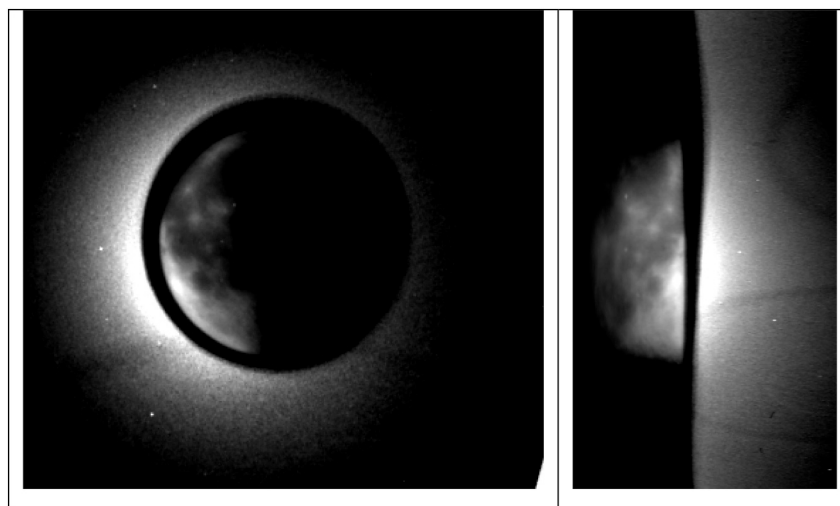

Fig. 1. (a) Sodium corona observed on February 7, 2018, with the image of the Moon superimposed on the occulting disk (left); (b) the polar transform of this image is on the right. The image was rotated so that north is up.
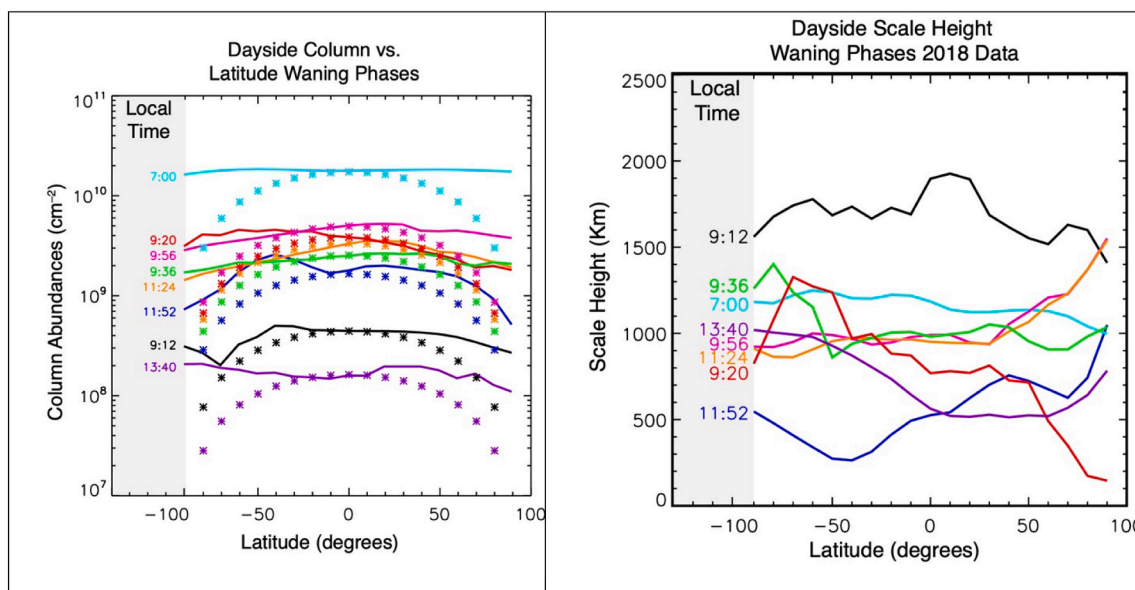
Fig. 2. (a) Dayside zenith column abundances of lunar sodium at the limb observed in 2018 are shown for waning phases. The local times at the limb are shown at the left. The observations are shown as solid lines while the asterisks are a cosine function normalized to the observation at the equator. The intensity is greatest in the early morning. (b) Scale heights are shown at right. The average scale height is 900–1000 km.

Table 2
Data for waxing phases 2018.

Date (2018)	Phase angle (°)	Local time at limb	Col. abund. eq. (cm^{-2})	Peak col. abund (cm^{-2})	Location peak (lat)	Color in Fig. 3
Jan 23	113	10:30	6.7×10^8	1.5×10^9	+50	blue
Jan 24	101	11:27	1.8×10^9	1.9×10^9	±10	magenta
Feb. 1	7	17:30	1.8×10^{10}	2.2×10^{10}	+70	army green
Feb 24	81	12:36	3.2×10^9	3.2×10^9	±10	purple
Feb 26	54	14:24	6.8×10^9	7.0×10^9	+20	lt. grey
Feb 27	40	15:33	8.0×10^9	8.5×10^9	+30	dk. grey
Mar 28	40	15:20	2.8×10^9	3.2×10^9	+30	black
Mar 29	32	15:52	1.5×10^9	2.2×10^9	−10	red
Dec 20	36	15:36	1.8×10^8	2.2×10^8	−50	lt. blue
Dec 21	23	16:28	1.9E9	2.4E9	+90	aqua

limb for each of these observations, but we do not see any correlation with surface brightness due to local continuum subtraction. Our observations are shown as solid lines. A cosine latitude function, normalized to the equatorial intensity at that date, is shown as asterisks with the same color as the corresponding date of observation. This shows that the data are not strictly symmetric about the equator nor do column abundances follow a $\cos^2$ function of latitude as expected from theory (e.g. Sarantos et al., 2010), or a $\cos^3$ functional form as found by Potter and Morgan (1998). The highly asymmetric N/S sodium profile seen at many lunar phases is consistent with observations published by Potter and Morgan (1991) where they report a D_2 emission intensity at an altitude of 50 km of ∼0.45 kR at the west limb, 1.0 kR at the north limb, 2.0 kR at the south limb and 1.5 kR at the east limb, on Feb. 21, 1989. We often see N/S asymmetries of a factor of ∼2, consistent with Potter and Morgan (1991).

The column abundance observed for waning phases in 2019

decreases from 7 AM until early afternoon where observations ceased. The three observations with the highest column abundances are near Full Moon, Phase Angle (PA) 7°, or associated with increased ion flux to the surface (see Section 3.2).

The scale heights are consistent throughout 2017–2019, giving average scale heights about 1000 km (4500 K), but sometimes as low as 500 km (2250 K) or as high as 2000 km (9000 K). The scale height data were smoothed in IDL using a smoothing factor of 3 since they tend to be noisy. Large scale heights at high latitudes may be spurious since they correspond to low density regions. Since we observe above about 140 km from the surface, these scale heights probably represent the tail of a distribution function and not the source itself, but it does indicate that a large component of the exosphere is escaping (Killen et al., 2018).

Our measured scale heights, varying from roughly 800 to 1800 km (3600 K < T < 8100 K), are broadly consistent with Kuruppuaratchi et al. (2019) and with the data set published in Killen et al. (2019). Although the intensity extrapolated to the surface decreases with latitude, the scale height increases with latitude, so that the exospheric column decreases more slowly with increasing latitude than does a cosine function. Mendillo et al. (1993) reported scale heights for the extended Na exosphere that agree with ours, particularly for waxing phases: a sodium scale height of approximately 1000 km (T = 4500 K) near the equator increasing to >2000 km (T = 9000 K) at the poles. Potter and Morgan (1991) reported temperatures of 1150 K at the equatorial limb, and 450 K above the north pole, both lower than our measured temperatures. However, the Potter and Morgan (1991) scale height is based on observations taken solely within 300 km of the lunar surface. Our observations begin at about 150 km above the lunar surface and extend to about 1700 km. These disparate scale heights would be consistent with two different populations. Two-temperature exospheres have been found elsewhere, notably H at Mercury below 300 km fits a 110 K profile; at higher altitudes the exosphere fits a 420 K profile (Broadfoot et al., 1976; Vervack et al., 2018). Because of thermal loss of this low mass atom, and without thermally re-accommodating to the surface, the exosphere retains only the low speed particles from the initial distribution. There is no process to fully repopulate the high energy tail. Thus, the distribution is no longer accurately described by a thermal population but mimics a two-component distribution.

Our measured scale heights are generally least at noon (PA 90°), increasing toward the morning and evening terminators, unlike those
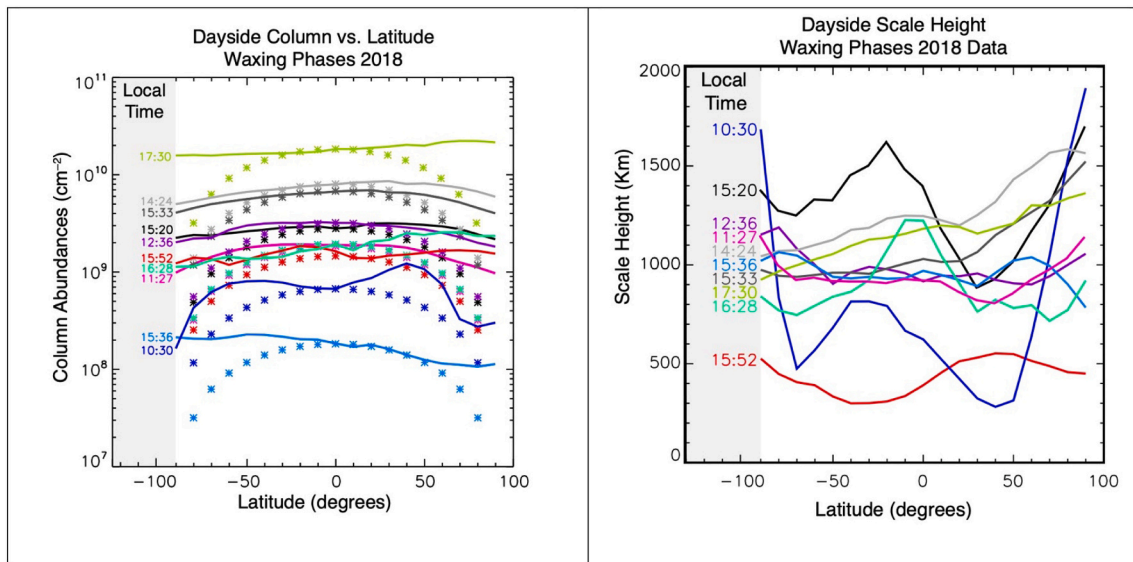
Fig. 3. (a) Dayside column abundances (atoms cm^{-2}) of lunar sodium at the limb are shown (solid lines) for waxing phases for 2018 data. (b) Scale heights are shown on the right with the same color scale.

Table 3
Data for phases 2019.

Date (2019)	Phase angle	Local time at limb	Col. abund. equator (cm^{-2})	Peak col. abund. (cm^{-2})	Location peak (latitude)	Color in Fig. 4
Apr. 2	150	16:00	2.7×10^8	6.2×10^8	+90	magenta
Apr. 25	68	10:30	2.76×10^9	2.8×10^9	−10	red
Apr. 27	90	12:00	6.5×10^8	6.7×10^8	−10	orange
June 15	28	16:08	5.2×10^9	9.2×10^9	+90	grey
June 22	53	9:30	3.6×10^9	3.7×10^9	+20	purple
June 23	64	10:00	2.1×10^9	2.2×10^9	−10	black
June 24	74	11:00	7.9×10^8	8.7×10^8	−20	green
June 25	85	11:40	2.0×10^9	2.0×10^9	+10	blue

measured by Potter and Morgan (1991) for lower altitude observations. Observed scale heights increase as the Moon approaches full phase, as previously reported, but also as it approaches new Moon. This result is consistent with Potter et al. (2000), who reported scale heights at lunar phases 4.4° and 76.2°. They concluded that the sodium temperature increases with decreasing phase angle. We show that the pattern repeats as the phase angle increases from 90° to 180°. This appears to imply that the scale height increases when the observer is looking over morning and evening terminators.

When reduced to surface number density or column abundance, the values are consistent with previous work. The uncertainty is increased when we observe sodium within ~15° of full moon due to the increased light scatter off the limb, as shown in Killen et al. (2019).

3.2. Ion effects

Dates with an exceptionally high abundance are associated with high ion flux in the magnetosheath (March 3, 2018, Feb. 26 & 27, 2018), or near Full Moon (Feb. 7) (Table 4). We obtained ion fluxes at the Moon from the ARTEMIS ElectroStatic Analyzer (ESA) data (McFadden et al.,

2008). The ion fluxes abruptly increase mid-day on March 3, 2018, as the Moon entered the magnetosheath as measured by the ARTEMIS ESA (Fig. 5), along with the lunar sodium exospheric column abundances (Table 1 and Fig. 2). As ARTEMIS does not measure ion composition, we cannot determine the ion composition with certainty. Periods when the Moon is fully in the magnetosheath are generally dominated by protons with some contribution from solar wind alphas. When crossing into the boundary layer and magnetosphere, it is possible that heavier ions may be present (e.g., Seki et al., 1998; Poppe et al., 2016); however, we have inspected the ion fluxes for both of the periods in question and do not find obvious evidence of heavy ion beams similar to those described in either Seki et al., 1998 or Poppe et al., 2016. Potter and Morgan (1991) concluded that ion impact is not an important factor in producing the sodium exosphere because the column abundance changed very little when the Moon was shielded from the solar wind while inside the Earth's magnetotail. This conclusion is based on the assumption that there is no ion flux to the lunar surface while the Moon is inside the magnetosheath and magnetotail; however, in-situ ARTEMIS observations have demonstrated that ion flues in the magnetotail, while reduced in magnitude compared to the solar wind, do not fall to zero (and in particular, can *increase* for ion energies greater than ~10 keV) (e.g., Poppe et al., 2018).

Other dates with a high column abundance of sodium, January 30 - Feb. 1, 2018, do not have enhanced ion flux at the Moon (Fig. 6). As the Moon exited the magnetosheath, the ion flux in the magnetotail varied between about 1.x10^5–1. x10^6 cm^{-2} s^{-1}. This variability is due to the Moon transiting through the lobes (where ion flux tends to be ≦1.x10^5 cm^{-2} s^{-1}) and either the plasma sheet or boundary layer (where fluxes are ~1. x10^6 cm^{-2} s^{-1}). However, ion flux was high on January 29, when the Moon was in the magnetosheath, the day before the column abundance enhancement was measured. Therefore the effects of high ion flux, and hence sputtering, may have persisted for two days. The mass of the Na exosphere is expected to return to the pre-high-ion-flux regime by two days after the enhanced ion flux ended (Killen et al., 2012), but may have persisted longer. On January 30, the Na exosphere column abundance was about one fourth of the value for the high ion flux cases, consistent with a ten hour e-folding time expected from a high ion flux. For the March 3rd event, the ion flux increased by two orders of magnitude, while the column abundance increased by one order of magnitude. According to Schmidt et al. (2012), at Mercury 2% of the Na atoms ejected by Photon-Stimulated Desorption (PSD) escape due to
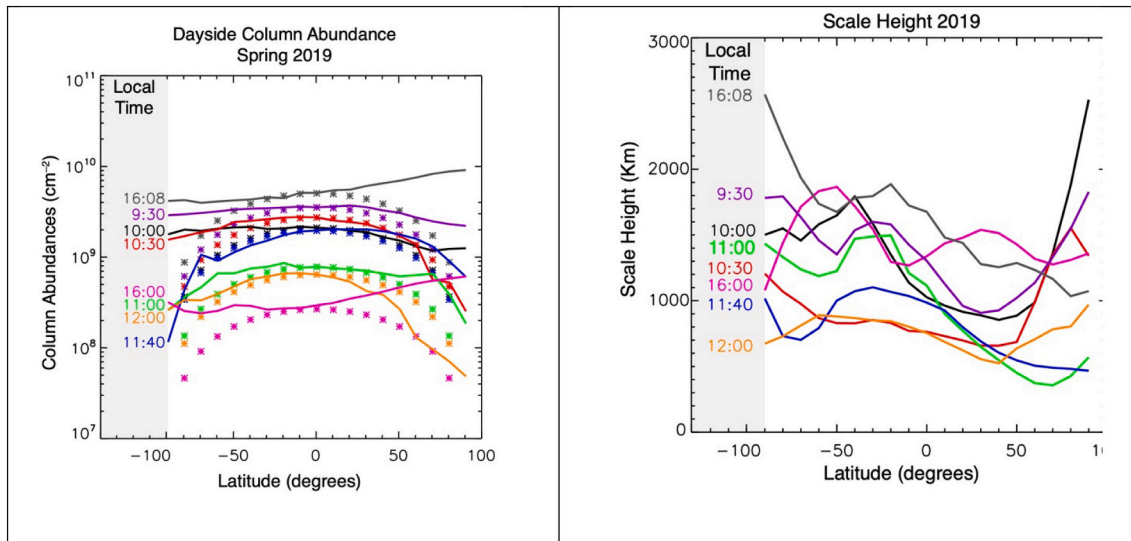
Fig. 4. (a) Column abundances measured at waning phases in the spring of 2019 are consistent with waning phases observed in 2018. For waning phases, column abundance is greatest in early morning and decreases throughout the day. Only one of these observations (at 16:08) was waxing phase, 28°, and this date has a similar local time as that at phase 150° (the one at 16:00) but the waxing phase at local time 16:08 (28°) is near full moon and the waning phase at local time 16:00 (PA 150°) is observed near new moon. (b) Scale heights are shown on the right with the same color scheme.

Table 4
Dates of high ion flux, Phase angle, Column Abundances, and ion flux.

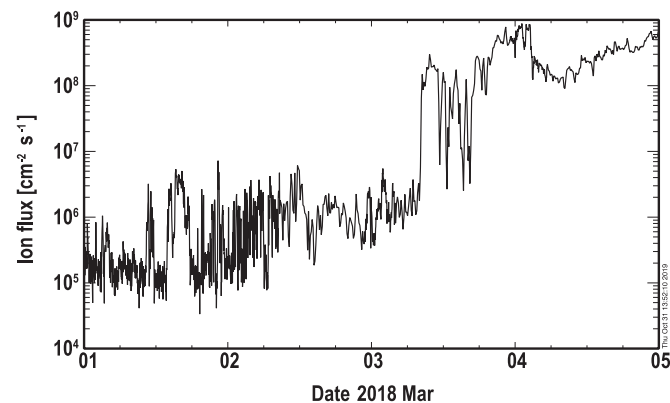| Date (2018)	Phase angle (degrees)	Column abund. equator (cm^{-2})	Ion flux (cm^{-2} s^{-1})	Wax/ Wan
Mar. 3	14	1.7×10^{10}	5×10^8	Wan
Feb. 1	7	$2.x10^{10}$	2.5×10^6	Wax
Feb. 26	54	6.8×10^9	2.5×10^8	Wax
Feb. 27	40	$8.x10^9$	1.4×10^8	Wax

Fig. 5. ARTEMIS ESA data for March 01–March 05, 2018, showing an abrupt increase in ion flux at the Moon on March 3, when our measured column abundance was the largest we ever observed.

their kinetic energy but roughly 89% of the sputtered Na atoms escape. The mean speed of sputtered Na atoms is at least 10 km/s (depending on the velocity distribution assumed), whereas the escape velocity at the Moon is 2.4 km/s. Therefore most sputtered sodium atoms are on escape trajectories (Killen et al., 2018). We can conclude that if sputtering increased by two orders of magnitude, but >90% of those sputtered atoms escaped immediately, the increase in exospheric neutrals due to sputtering would be approximately one order of magnitude, as observed.
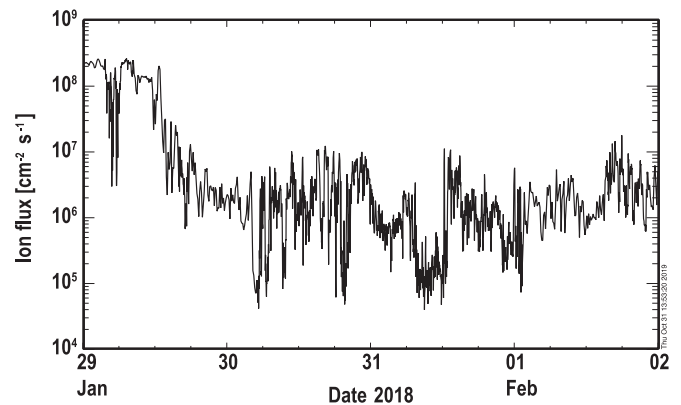

Fig. 6. Ion fluxes onto the Moon measured by the ARTEMIS ESA, January 29–February 2, 2018.

4. Conclusions

Data taken during the 2018–2019 time frame indicate that lunar zenith sodium column abundances vary from approximately 3×10^8 cm^{-2} to 1.7×10^{10} cm^{-2}. The data are consistent with a minimum near noon (first and third quarter) and maxima at the terminators (near Full Moon and New Moon). The 2017 data also clearly showed that the observed column abundance is smallest near noon and greatest at the morning and evening terminators. Szalay and Horanyi (2015) found, based on LADEE LDEX data, that the impacts of interplanetary micrometeoroids peak at dawn and decline with increasing time of day. However, our data indicate that both dawn and dusk terminators show increased column abundance relative to noon, and that the high latitude column abundances are similarly enhanced. This morphology was predicted and simulated by Smyth and Marconi (1995) and attributed to radiation pressure acceleration of Na atoms anti-sunward.

The observation on Feb. 1 2018, at PA 7° was taken near Full Moon and has a column abundance of 2×10^{10} cm^{-2}, nearly uniform in latitude. This observation shows the exosphere at the terminators (i.e. dawn and dusk). Potter et al. (2000), reported a column abundance a factor of 40 less than our Feb. 1 2018, result at a similar phase angle. They

reported a column of 5×10^8 cm^{-2} at a lunar phase of 4.3 and a scale height of 700 km. We reported a scale height of 1200 km. The difference in scale height alone cannot account for the factor of 40 difference between the two column abundances. This can be seen as evidence for ion-sputtering as an important source process, but one that is highly sporadic. Uncertainties are expected to be 50% near full Moon (Killen et al., 2019), but the difference is much larger than the uncertainty.

The highest measured column abundances correlate with increased ion flux to the surface, especially during the entrance of the Moon into the Earth's magnetosheath, presumably due to ion-sputtering. For the March 3 event, the Moon transited from the magnetotail into the magnetosheath, and the ion fluxes at the Moon as measured by the ARTEMIS ESA (Angelopoulos, 2010; Sibeck et al., 2011) abruptly increase, along with the lunar sodium exospheric densities (PA 14 in Fig. 2 and Table 1). This is consistent with the large residual Doppler widths measured with a Fabry-Perot spectrograph (Sarantos et al., 2018) that also correlate with the ion flux measured by ARTEMIS. These findings suggest a non-negligible contribution by sputtering. It was previously shown that the scale height of the sodium exosphere increased when the Moon was in the Earth's magnetosheath (Potter et al., 2000). Our results are consistent with that observation. The column abundance appears to be maximum at dawn and dusk and minimum at about noon, consistent with the effects of radiation pressure (Smyth and Marconi, 1995). The large scale height at the limb is not necessarily indicative of temperature of the source process, but possibly of radiation acceleration.

Observations using this coronagraph were previously published for the year 2017 (Killen et al., 2019). The key findings for that dataset were that the latitudinal variation in column abundance in the lunar exosphere does not follow any $\cos(\psi)$ function, where ψ is the angle from the subsolar point. The column abundances that we have derived from the data set taken in 2018–2019 decrease more slowly than a $\cos(\psi)$ function of latitude, in agreement with the 2017 data. For the 2018–2019 dataset, the peak Na abundance is most often in the southern

hemisphere for phase angles $<90°$, but waning phases peak closer to the equator. We do not see any correlation with underlying albedo differences. The north/south asymmetry is not as clear in terms of PA for the 2017 dataset.

Our data are all obtained above 140 km altitude. Thus we are not able to definitively conclude whether the exosphere is simply expanding and contracting rather than increasing/decreasing in total abundance, or whether we observe a high temperature component of a two temperature exosphere. The extended Na exosphere exhibits a scale height consistent with impact vaporization at $T = 4500$ K, but may be due to a mix of different source processes (Hurley et al., 2018). The temperature derived from a scale height is only an approximate concept for a surface-bounded exosphere since the lower boundary (the surface) does not provide a Maxwellian velocity distribution.

Declaration of Competing Interest

None.

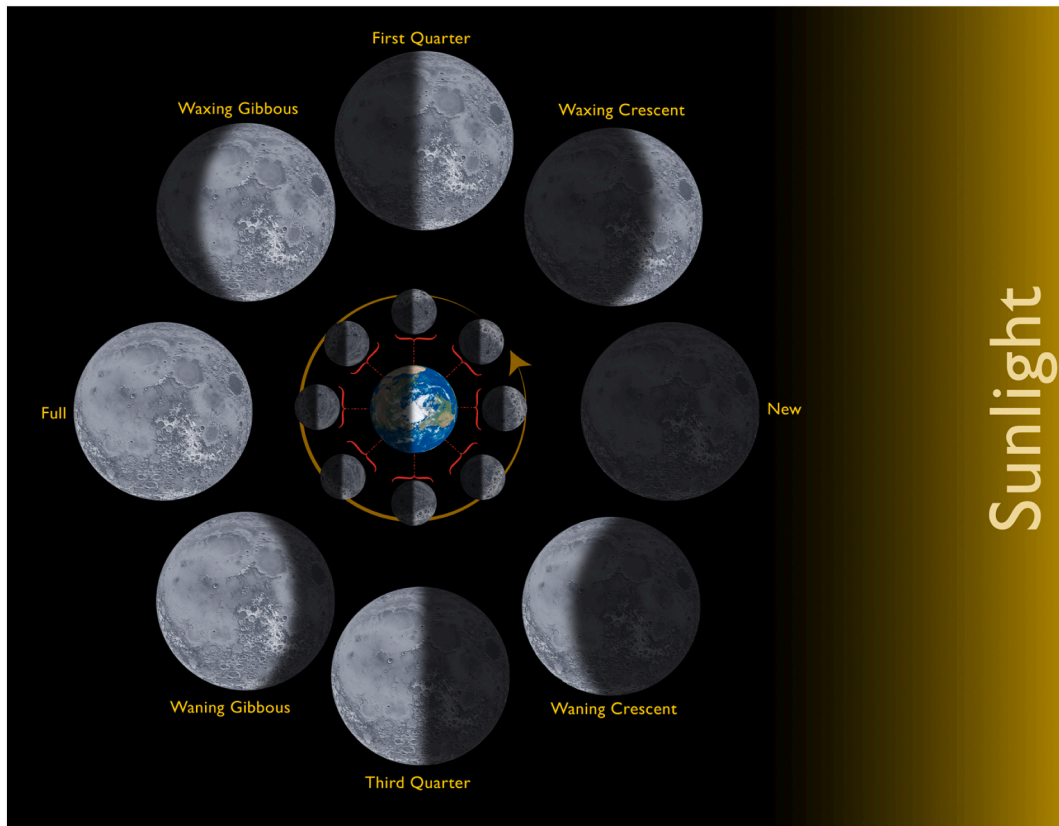## Acknowledgements

Appendix A. Appendix

Fig. A1. Lunar phases are illustrated here. Waxing phases are those from new Moon to full Moon. Waning phases are those from full Moon to new Moon. We observe the exosphere by placing an occulting disk over the Moon. We see the corona all the way around the limb, which includes the meridian from south to north through the equator at a time of day given by the tangent point of the line of sight from the Earth at the illuminated limb. The inner circle is the view from the north celestial pole, while the outer circle is the corresponding view from the Earth (northern hemisphere).

References

Angelopoulos, V., 2010. The ARTEMIS Mission. In: Russell, C., Angelopoulos, V. (Eds.), The ARTEMIS Mission. Springer, New York, NY.

Broadfoot, A.L., Shemansky, D.E., Kumar, S., 1976. Mariner 10: mercury atmosphere. Geophys. Res. Lett. 3, 577–580.

Chamberlain, J.W., Hunten, D.M., 1987. Theory of Planetary Atmospheres, 2nd ed. Academic Press, Inc., Orlando.

Hurley, D., Vervack Jr., R.J., Pryor, W.R., Killen, R.M., 2018. Hydrogen in mercury's exosphere: MESSENGER data and modeling. In: American Geophysical Union, Fall Meeting 2018, abstract #P22B-04, 2018AGUFM.P22B..04H.

Killen, R.M., Hurley, Dana, Farrell, William M., the DREAM Team, 2012. The effect on the lunar exosphere of a coronal mass ejection passage. J. Geophys. Res. 117 https://doi.org/10.1029/2011JE004011.

Killen, R.M., Burger, M.H., Farrell, W.M., 2018. Exospheric escape: a parametrical study. Adv. Space Res. 2017 https://doi.org/10.1016/j.asr.2017.06.015.

Killen, Rosemary M., Morgan, Thomas H., Potter, Andrew E., Plymate, Claude, Tucker, Roy, Johnson, Jamil D., 2019. Coronagraphic observations of the lunar sodium exosphere January - June, 2017. Icarus. https://doi.org/10.1016/j.icarus.2019.02.027.

Kuruppuaratchi, D.C.P., Mierkiewicz, E.J., Oliversen, R.J., Sarantos, M., Derr, N.J., Gallant, M.A., Rosborough, S.A., Freer, C.W., Salsbury, L.C., Gardner, D.D., Lupie, O. L., Roesler, F.L., 2019. High-resolution, ground-based observations of the lunar sodium exosphere during the lunar atmosphere and dust environment explorer (LADEE) mission. J. Geophys. Res. https://doi.org/10.1029/2018JE005717.

McFadden, J.P., et al., 2008. The THEMIS ESA plasma instrument and in-flight calibration. Space Sci. Rev. 141, 277–302.

Mendillo, M., Flynn, B., Baumgardner, J., 1993. Imaging experiments to detect an extended sodium atmosphere on the moon. Adv. Space Res. 13, 313–319. https://doi.org/10.1016/0273-1177(93)90085-P.

Poppe, A.R., et al., 2016. ARTEMIS observations of terrestrial ionospheric molecular ion outflow at the moon. Geophys. Res. Lett. 43.

Poppe, A.R., Farrell, W.M., Halekas, J.S., 2018. Formation timescales of amorphous rims on lunar grains derived from ARTEMIS observations. JGR Planets 123.

Potter, A.E., Morgan, T.H., 1991. Observations of the lunar sodium exosphere. Geophys. Res. Lett. 18, 2089–2092. https://doi.org/10.1029/91GL02621.

Potter, A.E., Morgan, T.H., 1998. Coronagraphic observations of the lunar sodium exosphere near the lunar surface. J. Geophys. Res. 103 (E4), 8581–8586. https://doi.org/10.1029/98JE00059.

Potter, A.E., Killen, R.M., Morgan, T.H., 2000. Variation of lunar sodium during passage of the moon through the earth's magnetotail. J. Geophys. Res. Planets 105, 15073–15084. https://doi.org/10.1029/1999JE001213.

Sarantos, M., Killen, R.M., Sharma, S.A., Slavin, J.A., 2010. Sources of sodium in the lunar exosphere: modeling using ground-based observations of sodium emission and spacecraft data of the plasma. Icarus 205, 364–374. https://doi.org/10.1016/j.icarus.2009.07.039.

Sarantos, M., Kuruppuaratchi, D., Mierkiewicz, E., 2018. New constraints on the Escape of Sodium and Potassium from the Moon, 42nd COSPAR Scientific Assembly, Abstract B3.1-69-18.

Schmidt, C.A., Baumgardner, J., Mendillo, M., Wilson, J.K., 2012. Escape rates and variability constraints for high-energy sodium at mercury. J. Geophys. Res. 117, 14. https://doi.org/10.1029/2011JA017217. A03301.

Seki, K., et al., 1998. Statistical properties and possible supply mechanism of tailward cold O^+ beams in the lobe/mantle regions. J. Geophys. Res. 103 (A3).

Sibeck, D.G., Angelopoulos, V., Brain, D.A., Delory, G.T., 29 others, 2011. ARTEMIS science objectives. Space Sci. Rev. https://doi.org/10.1007/s11214-010-9687-2.

Smyth, W.H., Marconi, M.L., 1995. Theoretical overview and modeling of the sodium and potassium atmospheres of the moon. Astrophys. J. 443, 371–392.

Szalay, J.R., Horanyi, M., 2015. Annual variation and synodic modulation of the sporadic meteoroid flux to the Moon. Geophys. Res. Lett. 42, 24. https://doi.org/10.1002/2015GL066908.

Vervack, R.J., Hurley, D.M., Pryor, W., Killen, R.M., 2018. MESSENGER orbital observations of mercury's hydrogen exosphere. In: Presented at Mercury: Current and Future Science of the Innermost Planet, Columbia, Md., May 1–3.